Novel Nickel- and Magnesium-Modified Cenospheres as Catalysts for Dry Reforming of Methane at Moderate Temperatures

Bogdan Samojeden [1],*[iD]**, Marta Kamienowska** [1,2]**, Armando Izquierdo Colorado** [2]**,
Maria Elena Galvez** [2][iD]**, Ilona Kolebuk** [1]**, Monika Motak** [1] **and Patrick Da Costa** [2],*

[1] AGH University of Science and Technology, Al. A. Mickiewicza 30, 30-059 Kraków, Poland; kamienowska@agh.edu.pl (M.K.); kolebuk@student.agh.edu.pl (I.K.); motakm@agh.edu.pl (M.M.)

[2] Institut Jean Le Rond D'Alembert, Sorbonne Université, 2 place de la Gare de Ceinture, 78210 Saint-Cyr- L'École, France; armandoley35@gmail.com (A.I.C.); elena.galvez_parruca@upmc.fr (M.E.G.)

* Correspondence: Bogdan.Samojeden@agh.edu.pl (B.S.); patrick.da_costa@sorbonne-universite.fr (P.D.C.); Tel.: +48-126172123 (B.S); +33-130854862 (P.D.C.)

Abstract: Cenospheres from coal fly ashes were used as support in the preparation of Ni–Mg catalysts for dry reforming of methane. These materials were characterized by means of XRD, H_2-temperature-programmed reduction (H_2-TPR), CO_2-temperature-programmed desorption (CO_2-TPD), and low-temperature nitrogen sorption techniques. The cenosphere-supported catalysts showed relatively high activity and good stability in the dry reforming of methane (DRM) at 700 °C. The catalytic performance of modified cenospheres was found to depend on both Ni and Mg content. The highest activity at 750 °C and 1 atm was observed for the catalyst containing 30 wt % Mg and 10, 20, and 30 wt % Ni, yielding to CO_2 and CH_4 conversions of around 95%.

Keywords: cenospheres; magnesium; nickel; dry reforming of methane; H_2/CO production

1. Introduction

The policies of the European Union, with new laws and regulations which aim to protect the environment, have led to increased interest in finding new and efficient applications of coal combustion products. Currently, the total annual production of coal fly ash is around 780 million tons worldwide [1], which makes it necessary to carry out detailed studies on its alternative applications [2–4]. Cenospheres, present in fly ash, are hollow particles of about 10–1000 μm in diameter, with a density lower than 1 g/cm³ [5]. These could become catalyst supports for certain chemical processes that require high thermal stability [6,7]. Cenospheres are composed of a mixture of aluminosilicates with some amount of K, Ca, Fe, Mg, and a small addition of Ti, Na, P, S, and trace elements [7]. Because of the high amount of Al_2O_3 (23%–33%) and the fact that they were formed at temperatures over 1200 °C, cenospheres have high mechanical and thermal strength, and thus have potential applications in many branches of industry [8]. Cenospheres were examined and have exhibited positive results as catalysts, for example, for esterification of n-octanol with acetic acid [6], for deNOx processes [9], as well as in practical uses in the degradation of pollutants or for water cleanup [10]. Additionally, it was concluded that when used as catalysts, they can show high conversion and selectivity for some important organic reactions under solvent-free conditions [11].

Apart from the problem of solid waste, another important issue connected with energy production from fossil fuels is the high emission of carbon dioxide. The increase of CO_2 concentration in the atmosphere is considered to be the main reason for climate change [12]. Utilization and transformation

of methane and carbon dioxide into valuable chemicals could be an interesting alternative to CO_2 sequestration [13]. Jeong et al. [14] tested catalysts based on Pd in catalytic oxidation of methane. Additionally, Zhang et al. [15] showed that bimetallic alloyed $Pt_{71}Co_{29}$ catalysts exhibited high activity for methanol oxidation reactions. Torimoto et al. [16] tested Ni, Pt, Pd, and Rd catalysts in steam reforming of methane. The low-temperature heterogeneous catalytic reactions for hydrogen production are enabled with very high yield. Mota and Kim [17] described promising features of Ni-, Co-, and Fe-based catalytic systems on CO_2 reduction reactions (CO_2RR), namely thermochemical, electrochemical, and photochemical. Thermochemically driven CO_2RR has significant potential to be applied on a large scale.

The dry reforming of methane (DRM) is a chemical process that converts CH_4 and CO_2 to syngas with a H_2/CO ratio of 1, which can be directly used in many important chemical reactions, among them Fischer–Tropsch synthesis [18–21].

The main reaction ($CH_4 + CO_2 = 2CO + 2H_2$) is efficient at temperatures higher than 730 °C, and is accompanied by several side reactions, among which the Boudouard reaction ($2CO = C + O_2$) and methane decomposition are especially responsible for carbon deposit formation during DRM [22]. This process has not as yet been applied on an industrial scale due to some complications connected with catalyst deactivation (carbon deposition formation) [18,22,23]. However, Linde and BASF installed the Pilot Plant in Wilsonville, Alabama, USA in 2015 [24]. The catalysts that have been most often examined for dry reforming of methane are nickel, ruthenium, and rhodium [18,25], supported on different carriers.

Although the noble metals are more resistant to carbon deposition, as well as more active than nickel, they are more expensive and less available. For this reason, in order to allow the DRM to become a fully mature industrial process, there is a need to develop a Ni-based catalyst which is more active and more stable, as well as low-cost and eco-friendly [26]. To the best of our knowledge, no studies concerning the use of cenospheres as catalysts for dry reforming of methane have been reported in the literature. These cenospheres as by-products of fly ashes are characterized by their high thermal stability [23,27,28], which is important for high-temperature processes such as reforming (steam, dry, oxy, etc.). Thus, the aim of this work was to use these cenospheres as supports for catalysts in DRM. Moreover, although the role of Mg in DRM is not yet fully clear, several reports (e.g., that of Dębek et al. [29]) have claimed that the high Lewis basicity of MgO has a beneficial effect, since CO_2 adsorption is enhanced on basic support. Thus, in this work, in order to improve the basicity of the studied catalysts, cenospheres were modified with MgO in addition to Ni.

2. Results and Discussion

2.1. Catalyst Characterization

Figure 1 shows XRD patterns of calcined and spent materials. XRD patterns for the calcined samples showed reflections at 2θ of 62° and 74° assigned to MgO, and at 2θ of 37°, 43°, and 75° arising from NiO. For the reduced catalysts, reflections at 2θ equal to approximately 44°, 51°, and 76° from metallic nickel are visible in all examined catalysts. The crystallite sizes calculated from the Scherrer equation range from 29 to ~50 nm, as presented in Table 1, and are higher than for some other supported Ni-catalysts reported in the literature, such as Ni/Mg/Al hydrotalcite-derived materials [30] or Ni/Ce/Fe clay-based samples [31]. For the catalysts studied here, there is greater Ni content of 20%–30% as compared to 10%. However, the crystallite sizes for the catalysts studied in this work were smaller than those reported in the literature for 11% $NiO/CaAl_2O_4$ catalysts (65 nm) [32].
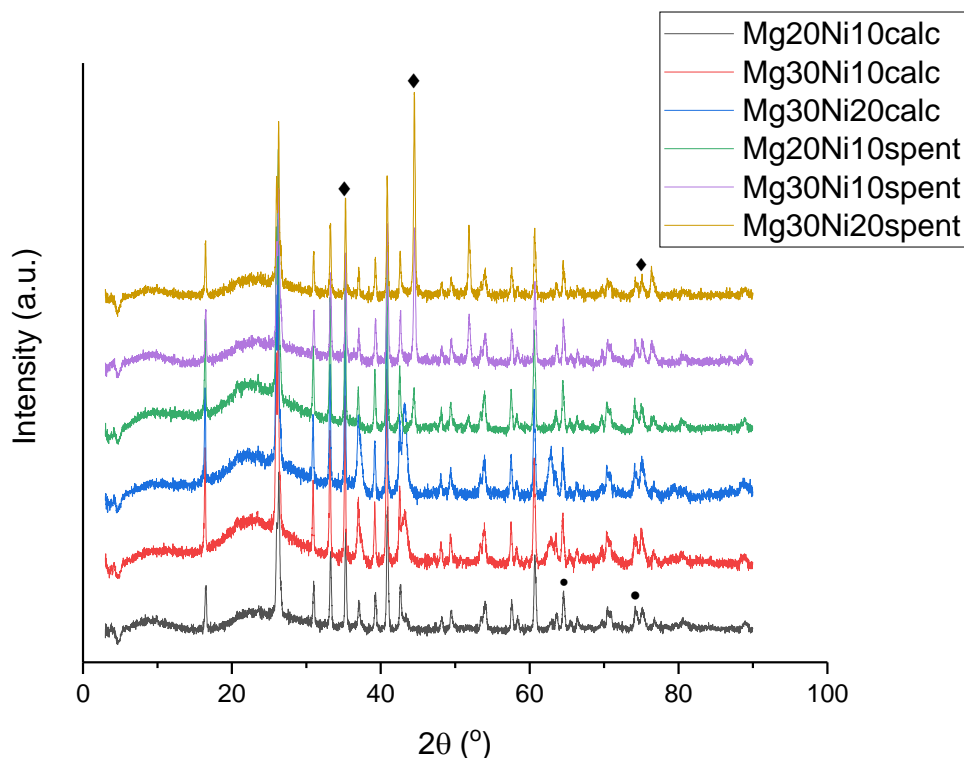
Figure 1. XR diffractograms of calcined and spent catalysts.

Table 1. Specific surface area (S_{BET}) of the calcined samples, H_2 consumption and basicity of the calcined and spent catalysts, and crystallite size of Ni° particles for the reduced and spent modified cenosphere catalysts.

	Ni	S_{BET}	H_2 Consumption for the Calcined Samples	Basicity for the Calcined Samples after Reduction *	Basicity after DRM *	Nickel Crystallite Size for the Reduced Samples **	Nickel Crystallite Size for the Spent Catalysts **	Carbon Deposi-tion [†]
	wt %	m²/g	μmol_{H2}/g_{cat}	μmol_{CO2}/g_{cat}	μmol_{CO2}/g_{cat}	nm	nm	%
Mg10								
	10	1	53.4	35.0	29.0	20	23	0.5
	20	1	201.5	30.0	44.7	40	41	0.6
	30	2	455.5	27.1	28.1	36	39	0.9
Mg20								
	10	1	82.86	29.7	19.6	23	24	-
	20	2	344.8	22.3	41.5	44	31	-
	30	4	947.5	18.3	21.5	43	41	-
Mg30								
	10	2	233.7	19.9	36.0	32	34	-
	20	4	386.2	48.0	49.3	39	41	1.1
	30	4	612.3	26.0	35.9	36	37	-

* measured by CO_2 TPD as reported elsewhere [22]; ** calculated from XRD by the Scherrer equation; [†] evaluated from TG Analysis.

Temperature-programmed reduction (H_2-TPR) profiles for the catalysts after calcination are presented in Figure 2. A single symmetric reduction peak assigned to the reduction of nickel oxide is visible from 280 °C to 420 °C, with the maximum at ~350 °C, which is in good agreement with the literature [33,34]. For the catalysts with a loading of 30% Mg and the lowest nickel content, a shift to higher reduction temperatures can be observed, which may indicate stronger interactions between the support and the active phase [30,35].
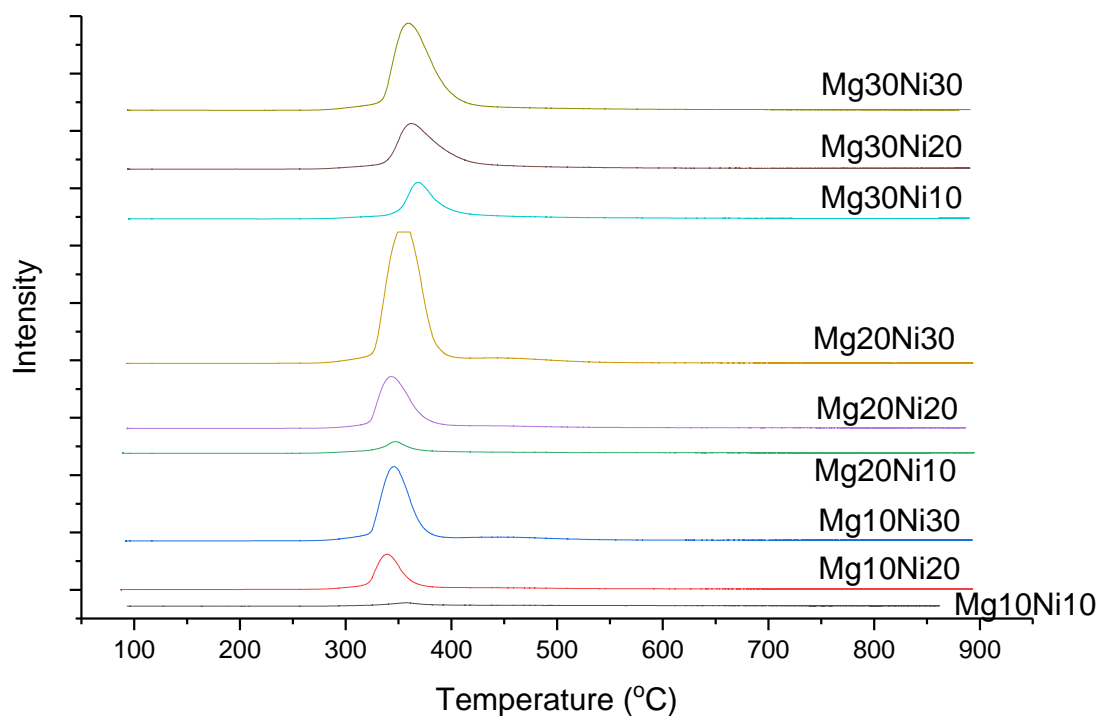
Figure 2. Temperature-programmed reduction (H_2-TPR) profiles of calcined catalysts.

H_2 consumption (Table 1) increased with the loading of Ni and Mg, with the exception of Mg30Ni30 as compared to Mg20Ni30. It should be mentioned, however, that H_2 consumption is rather low in comparison to some catalysts reported in the literature, for example, for 10 wt % Ni/CZ/SBA-15 (1634 µmol/g) [19] or 15 wt % Ni-Ce-Fe clay (1470 µmol/g) [31]. The obtained values in Table 1 are close to the ones that were reported for mixed oxides derived from double-layered hydroxides containing ~20% Ni and ~30% Mg [36].

The latter result indicates a lower reducibility of the microsphere-supported catalysts, possibly due to stronger interaction between NiO and MgO/microspheres.

A CO_2 temperature-programmed desorption (TPD) experiment was conducted to determine the basicity of the studied cenosphere catalysts. The results are reported in Table 1. The basicity of the calcined samples is relatively low, from ~18 to ~48 µmol/g, in comparison to some catalysts reported in the literature, for example, nickel contacting layered double hydroxide-derived catalysts with a basicity of around 130 µmol/g for Ni/La/Mg hydrotalcite [37] or 201 µmol/g for Ni/MgO-ZrO$_2$ [38], 350 µmol/g for 12 wt % Ni/KIT-6, and 190 µmol/g for (12 wt % Ni, 8 wt % Y)/KIT-6 [39].

This may be assigned to the lower specific surface areas of our studied catalysts.

2.2. DRM Catalytic Tests

Figure 3 presents results for catalytic tests for the obtained samples. One can note that the conversions of CO_2 and CH_4 increase with the temperature, and that at 750 °C, the conversions of CH_4 and CO_2 are both higher than 93%, and the H_2/CO is 0.98. For the sake of comparison, the supports were tested in DRM as a function of the temperature, and at 750 °C, and no significant activity was found.
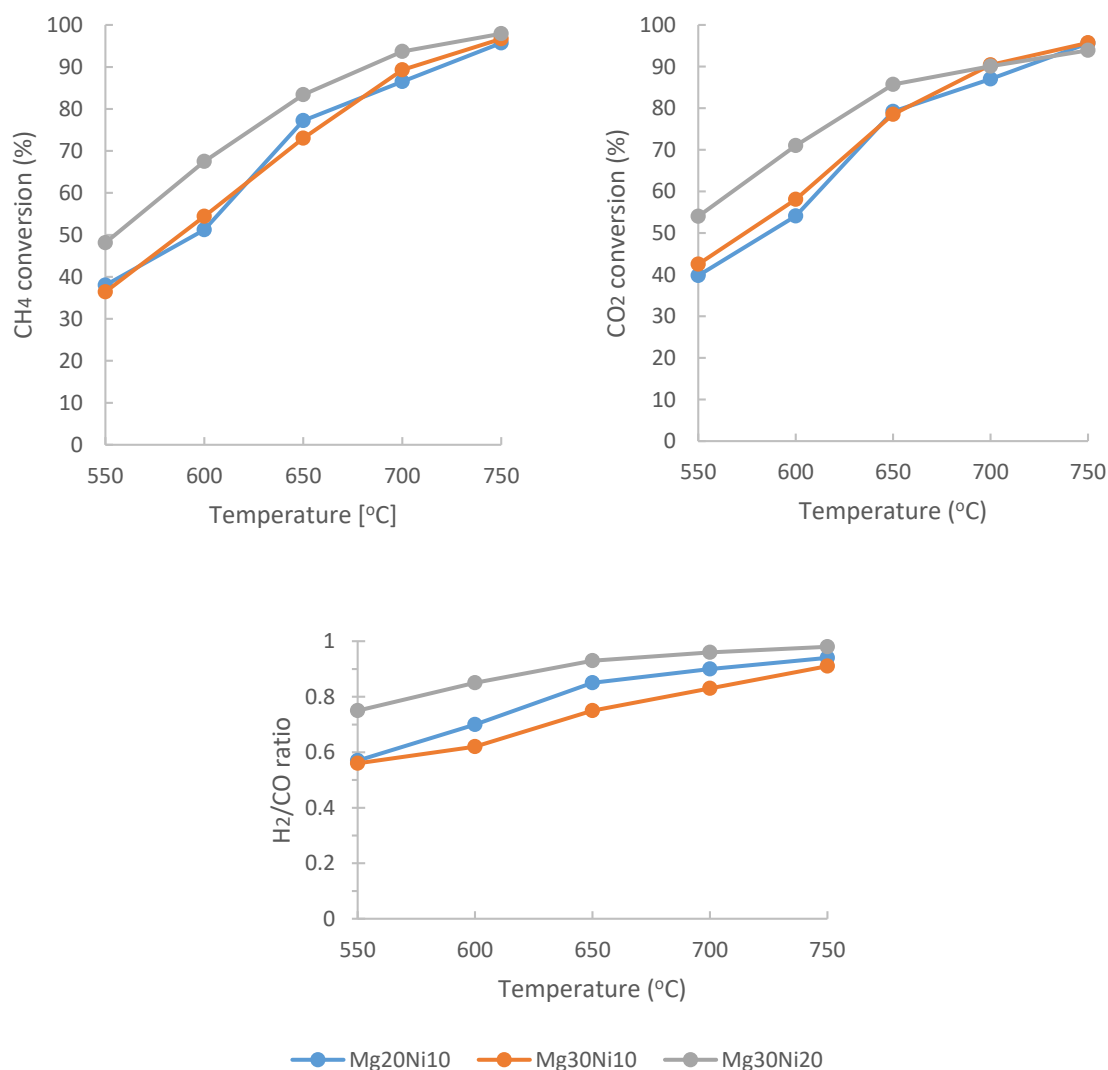
Figure 3. Catalytic tests of Mg20Ni10, Mg30Ni10, and Mg30Ni20 as functions of the temperature, 100 mL/min $CH_4/CO_2/Ar$ = 1/1/8.

In addition, activities in CO_2, CH_4, and H_2/CO increased with the increase in Ni content, to an extent depending on the Ni/Mg ratio. This may be ascribed to the stronger metal support interaction, as well as to a higher stabilization of NiO species [40].

Thus, it can be concluded that both CO_2 and CH_4 conversions and H_2/CO ratios depend on the Ni/Mg ratio, which is in agreement with the work of Dębek et al. [35].

2.3. Stability Test

The Mg30Ni20 catalyst which presented the highest activity in DRM as a function of temperature was selected for isothermal runs at 700 °C after an initial reduction under hydrogen at 800 °C (Figure 3). Under isothermal steady-state conditions, only a slight deactivation was observed. CH_4 conversion decreased from 91.4% to 86.6%, and CO_2 conversion from 92.3% to 90.1%, while H_2/CO ratio decreased by 6.1% after 7 h runs (Figure 4).
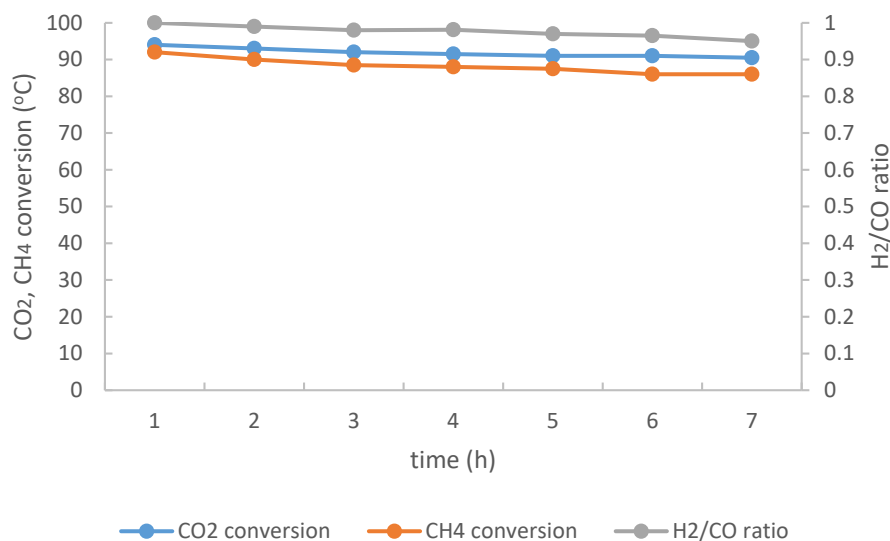
Figure 4. Stability test at 700 °C for 5 h under 100 mL/min $CH_4/CO_2/Ar = 1/1/8$ for Mg30Ni20.

2.4. Post-Test Characterization of the Catalysts

Our results for H_2-TPR, as well as the particle sizes of Ni crystallites for the samples after DRM, are summarized in Table 1. H_2 consumption indicates that a small amount of NiO was present after DRM. The presence of this reduction peak in the spent catalysts may point out that Ni particles were repeatedly oxidized and reduced during DRM process [35,41] (Table 1).

The XRD patterns for the catalysts after the DRM catalytic tests showed reflections of Ni^0 with the exception of Mg10Ni10 (Figure 1). Nickel crystallite sizes, calculated from XRD for the spent catalysts, are reported in Table 1.

In comparison to the reduced catalysts, the sizes of Ni particles are similar, proving the lack of sintering during DRM. For Mg20Ni20 and Mg20Ni30 the size of the Ni particle even decreased, which may have been caused by some redispersion of Ni crystallites. Similar effects were already observed for other types of mixed oxides, catalyst promoted or not [30,42]. Although the literature indicates carbon deposition in the form of graphite after DRM reactions on several types of catalysts—such as hydrotalcite-derived samples modified with Ce [30] or SBA-15-supported nickel catalysts promoted by $Ce_{0.75}Zr_{0.25}O_2$ mixed oxide [19]—for the studied materials, graphite carbon deposits could neither be confirmed by XRD nor excluded because at the relevant 2θ (°) region, approximately 26°, reflections from $Al_XSi_YO_Z$ (mullite) and Al_2O_5Si (sillimanite) from microspheres are also present [5].

In order to confirm the presence of carbon, a thermogravimetric analysis was performed in air from 100 to 1000 °C (figure not shown). For Mg10Ni10, Mg20Ni10, Mg30Ni10, and Mg30Ni20, only traces of carbon deposits of 0.5%, 0.6%, 0.9%, and 1.1% were observed (Table 1).

Until now, cenospheres have not been studied in DRM. Table 2 compares the results with other catalysts. Catalysts with similar Ni content or similar reaction conditions were selected for comparison, results are fully comparable because the experiments were carried out under the same conditions, and the presented results were selected for the best catalysts. The cenospheres examined in this work obtained better catalytic results. Dębek et al. [43] obtained similar results for catalysts containing 20 wt % Ni. The only slight differences concern the H_2/CO ratio.

Table 2. Comparison of catalytic properties over other catalysts reported in the literature.

Catalyst	Ni Loading	Reaction Conditions				Conversion *			Ref.
		Temp. (°C)	CH_4/CO_2	GHSV (h^{-1})	TOS (h)	CH_4 (%)	CO_2 (%)	H_2/CO	
HTNi	20	750	1/1	20,000	1	85	82	1.1	[44]
HT-25Ni	19.57	750	1/1	20,000	0.5	97	90	1.2	[43]
HT	20	750	1/1	20,000	0.5	82.5	86.5	0.93	[41]
Mg20Ni20	20	750	1/1	20,000	0.5	97.9	93.9	0.98	This work
Mg30Ni20	10	750	1/1	20,000	0.5	95.7	93.7	0.97	This work
Mg30Ni20	20	750	1/1	20,000	0.5	96.7	93.8	0.91	This work

* results obtained for the best catalysts.

3. Materials and Methods

3.1. Ni/Mg Cenosphere Catalyst Preparation

White commercial cenospheres (~32 wt % of Al_2O_3 and ~53 wt % SiO_2) from Cenospheres Trade & Engineering S.A. (Radom, Poland) were tested as supports for DRM catalysts. Microspheres were modified first by wet impregnation with $Mg(NO_3)_2$, followed by the incipient wetness method using $Ni(NO_3)_2$, as described by Kolebuk and Samojeden [45]. We then introduced 10, 20, or 30 wt % of Mg onto the samples, and then 10 wt %, 20 wt %, or 30 wt % of Ni. Each impregnation step was followed by drying at 100 °C and subsequent calcination at 500 °C for 6 h [45]. The catalysts were designated as MgxNiy, where x and y are amounts of introduced Mg and Ni, respectively; for example, Mg10Ni10 denotes the white cenospheres modified with 10 wt % of Ni and 10 wt % of Mg.

3.2. Catalyst Characterization

XRD analysis was conducted to examine the structure and phase composition of the samples, as well as to determine Ni crystallite sizes before and after DRM catalytic tests. The average crystallite size of NiO was calculated from Ni reflection at ~44° using the Scherrer equation. The XRD Empyrean diffractometer from Panalytical (Almelo, UK), equipped with a CuKα radiation source ($\lambda = 0.154059$ nm), was used for these measurements.

The S_{BET} of the catalysts was determined by low-temperature N_2 sorption using a Belsorp Mini II apparatus (BEL, Osaka, Japan). Before each experiment, samples were degassed under vacuum for 3 h at 180 °C. To calculate the specific surface areas, the Brunauer–Emmett–Teller (S_{BET}) method was used.

Reducibility of the catalysts was evaluated by a temperature-programmed reduction (TPR) of H_2 (H_2-TPR) with a BELCAT-M (from BEL, Osaka, Japan), equipped with a thermal conductivity detector (TCD). The sample (~60 mg) was loaded into a quartz reactor, and prior to the TPR measurements it was pretreated at 100 °C for 120 min in flowing He. Then, a 5% (v/v) H_2/Ar gas mixture was introduced, and the catalyst was heated from room temperature to 900 °C at a rate of 7.5 °C/min, with a simultaneous measurement of hydrogen consumption.

The basicity of the catalysts was determined using CO_2-TPD with the BELCAT-M. The materials (~60 mg) were pretreated under He flow at 500 °C for 120 min and then cooled down to 80°C. Subsequently, a mixture of 10% (v/v) CO_2/He was introduced for 60 min. After adsorption, the sample was flushed with He for 15 min to desorb the physically adsorbed CO_2. Then the sample was heated up to 800 °C at the rate of 10 °C/min under He flow, and CO_2 desorption was measured by the TCD.

The thermogravimetric non-isothermal measurements were made using a DynTHERM Thermogravimetric Analyzer by Rubotherm in the air atmosphere (100–1000 °C).

3.3. Catalytic Tests

DRM activity tests were performed under atmospheric pressure in a U-shaped quartz microreactor under 100 mL/min with the following composition: $CH_4/CO_2/Ar = 1/1/8$ as function of temperature from 550 to 750 °C. For each temperature, the catalyst was kept for approximately 30 min, corresponding to steady-state measurements. Another DRM test was conducted at 700 °C for 7 h in order to favor

DRM and avoid carbon formation based on thermodynamics. A k-type thermocouple was used to control the temperature of the catalyst bed. The composition of the exhaust gas was analyzed by a micro gas chromatograph Varian-CP 4900 equipped with COX column and TCD detector. The total flow of the feed was equal to 100 cm^3/min, controlled by a series of mass-flow controllers (BROOKS) and corresponding to the GHSV of 12,000 h^{-1}. The mass of the catalyst depended on its bulk density, and the calculated value for all tested samples was around 200 mg. Prior to the reaction, the samples were reduced in situ at 800 °C for 1 h in 5% (v/v) H$_2$/Ar. The CO$_2$ and CH$_4$ conversion as well as the H$_2$/CO molar ratio of catalysts were calculated as follows:

$$X_{CH_4} = \frac{n_{CH_4,in} - n_{CH_4,out}}{n_{CH_4,in}} \times 100\%, \tag{1}$$

$$X_{CO_2} = \frac{n_{CO_2,in} - n_{CO_2,out}}{n_{CO_2,in}} \times 100\%, \tag{2}$$

$$H_2/CO = n_{H_2,out}/n_{CO,out}, \tag{3}$$

where X_{CH_4} and X_{CO_2} refer to the conversion of CH$_4$ and CO$_2$.

4. Conclusions

The presented study focused on the examination of cenospheres modified with nickel and magnesium as catalysts for the dry reforming of methane. The modification with Mg (in MgO form) and Ni resulted in high activity in the examined catalysts. CO$_2$ and CH$_4$ conversions increased with the rising amount of MgO and the increasing Ni/Mg ratio. This may be due to the favored support–metal interaction. The samples Mg20Ni10, Mg30Ni10, Mg30Ni20, and Mg30Ni30 were the most stable and active catalysts in all conducted experiments. Ni sintering was negligible after 7 h runs. These investigations on cenospheres modified with Mg and Ni proved that this type of material can be used as an effective, stable, and non-expensive catalyst in the DRM.

Conflicts of Interest: The authors declare no conflict of interest.

References

1. Lecomte, T.; Ferrería De La Fuente, F.J.; Neuwahl, F.; Canova, M.; Pinasseau, A.; Jankov, I.; Brinkmann, T.; Roudier, S.; Delgado Sancho, L. *Best Available Techniques (BAT) Reference Document for Large Combustion Plants-Industrial Emissions Directive 2010/75/EU (Integrated Pollution Prevention and Control)*; Publications Office of the European Union: Luxembourg, 2017; ISBN 978-92-79-74303-0.
2. Cuéllar-Franca, R.M.; Azapagic, A. Carbon capture, storage and utilisation technologies: A critical analysis and comparison of their life cycle environmental impacts. *J. CO$_2$ Util.* **2015**, *9*, 82–102. [CrossRef]
3. Wee, J.-H. A review on carbon dioxide capture and storage technology using coal fly ash. *Appl. Energy* **2013**, *106*, 143–151. [CrossRef]
4. Acar, I.; Atalay, M.U. Recovery potentials of cenospheres from bituminous coal fly ashes. *Fuel* **2016**, *180*, 97–105. [CrossRef]
5. Żyrkowski, M.; Costa, R.; Santos, L.F.; Witkowski, K. Characterization of fly-ash cenospheres from coal-fired power plant unit. *Fuel* **2016**, *174*, 49–53. [CrossRef]
6. Chandane, V.S.; Rathod, A.P.; Wasewar, K.L.; Sonawane, S.S. Efficient cenosphere supported catalyst for the esterification of n-octanol with acetic acid. *C. R. Chim.* **2017**, *20*, 818–826. [CrossRef]
7. Ranjbar, N.; Kuenzel, C. Cenospheres: A review. *Fuel* **2017**, *207*, 1–12. [CrossRef]

8. Fomenko, E.V.; Anshits, N.N.; Solovyov, L.A.; Mikhaylova, O.A.; Anshits, A.G. Composition and Morphology of Fly Ash Cenospheres Produced from the Combustion of Kuznetsk Coal. *Energy Fuels* **2013**, *27*, 5440–5448. [CrossRef]

9. Samojeden, B.; Drużkowska, J.; Duraczyńska, D.; Poddębniak, M.; Motak, M. Use of iron and copper-promoted cenospheres as catalysts in the selective catalytic reduction of nitrogen(II) oxide with ammonia. *Przem. Chem.* **2019**, *1*, 55–59.

10. Zhang, J.; Wang, B.; Cui, H.; Li, C.; Zhai, J.; Li, Q. Synthesis of CeO_2/fly ash cenospheres composites as novel photocatalysts by modified pyrolysis process. *J. Rare Earths* **2014**, *32*, 1120–1125. [CrossRef]

11. Hosseini Asl, S.M.; Ghadi, A.; Sharifzadeh Baei, M.; Javadian, H.; Maghsudi, M.; Kazemian, H. Porous catalysts fabricated from coal fly ash as cost-effective alternatives for industrial applications: A review. *Fuel* **2018**, *217*, 320–342. [CrossRef]

12. Samojeden, B. The current and future trends in chemical CO_2 utilization. In *Contemporary Problems of Power Engineering and Environmental Protection*; Pikoń, K., Czarnowska, L., Eds.; Silesian University of Technology: Gliwice, Poland, 2018; pp. 215–226. ISBN 978-83-950087-1-9.

13. Xu, L.; Song, H.; Chou, L. Ordered mesoporous MgO–Al_2O_3 composite oxides supported Ni based catalysts for CO_2 reforming of CH_4: Effects of basic modifier and mesopore structure. *Int. J. Hydrog. Energy* **2013**, *38*, 7307–7325. [CrossRef]

14. Jeong, M.; Nunotani, N.; Imanaka, N. Relationship between the conductivities of CeO_2-ZrO_2-MOx (M = Bi, Ca, Sn, Ni, Fe) solid solutions and catalytic activities during methane oxidation. *Bull. Chem. Soc. Jpn.* **2018**, *91*, 158–164. [CrossRef]

15. Zhang, L.; Zhang, X.F.; Chen, X.L.; Wang, A.J.; Han, D.M.; Wang, Z.G.; Feng, J.J. Facile solvothermal synthesis of $Pt_{71}Co_{29}$ lamellar nanoflowers as an efficient catalyst for oxygen reduction and methanol oxidation reactions. *J. Colloid Interface Sci.* **2019**, *536*, 556–562. [CrossRef] [PubMed]

16. Torimoto, M.; Murakami, K.; Sekine, Y. Low-temperature heterogeneous catalytic reaction by surface protonics. *Bull. Chem. Soc. Jpn.* **2019**, *92*, 1785–1792. [CrossRef]

17. Mota, F.M.; Kim, D.H. From CO_2 methanation to ambitious long-chain hydrocarbons: Alternative fuels paving the path to sustainability. *Chem. Soc. Rev.* **2019**, *48*, 205–259. [CrossRef]

18. Aramouni, N.A.K.; Touma, J.G.; Tarboush, B.A.; Zeaiter, J.; Ahmad, M.N. Catalyst design for dry reforming of methane: Analysis review. *Renew. Sustain. Energy Rev.* **2018**, *82*, 2570–2585. [CrossRef]

19. Albarazi, A.; Beaunier, P.; Da Costa, P. Hydrogen and syngas production by methane dry reforming on SBA-15 supported nickel catalysts: On the effect of promotion by $Ce_{0.75}Zr_{0.25}O_2$ mixed oxide. *Int. J. Hydrog. Energy* **2013**, *38*, 127–139. [CrossRef]

20. Duan, Y.; Shang, R.; Zhong, X.; Xie, W.; Wang, X.; Huang, L. In-situ synthesis of $NiMo_2C$/Al_2O_3 catalysts for dry reforming of methane. *Int. J. Hydrog. Energy* **2016**, *41*, 21955–21964. [CrossRef]

21. Yao, L.; Galvez, M.E.; Hu, C.; Da Costa, P. Mo-promoted Ni/Al_2O_3 catalyst for dry reforming of methane. *Int. J. Hydrog. Energy* **2017**, *42*, 23500–23507. [CrossRef]

22. Dębek, R.; Motak, M.; Galvez, M.E.; Grzybek, T.; Da Costa, P. Promotion effect of zirconia on Mg(Ni,Al)O mixed oxides derived from hydrotalcites in CO_2 methane reforming. *Appl. Catal. B Environ.* **2018**, *223*, 36–46. [CrossRef]

23. Abdullah, B.; Abd Ghani, N.A.; Vo, D.V.N. Recent advances in dry reforming of methane over Ni-based catalysts. *J. Clean. Prod.* **2017**, *162*, 170–185. [CrossRef]

24. BASF and Linde Successfully Complete Pilot Project at National Carbon Capture Center in Wilsonville, Alabama. Available online: https://www.linde-gaz.pl/pl/news_and_media/press_releases/news_20160719.html (accessed on 6 December 2019).

25. Şener, A.N.; Günay, M.E.; Leba, A.; Yıldırım, R. Statistical review of dry reforming of methane literature using decision tree and artificial neural network analysis. *Catalysis Today* **2018**, *299*, 289–302.

26. Dębek, R.; Wierzbicki, D.; Motak, M.; Galvez, M.E.; Da Costa, P.; Azzolina-Jury, F. Operando FT-IR study on basicity improvement of Ni(Mg,Al)O hydrotalcite-derived catalysts promoted by glow plasma discharge. *Plasma Sci. Technol.* **2019**, *21*, 045503. [CrossRef]

27. Damyanova, S.; Pawelec, B.; Arishtirova, K.; Fierro, J.L.G. Ni-based catalysts for reforming of methane with CO_2. *Int. J. Hydrog. Energy* **2012**, *37*, 15966–15975. [CrossRef]

28. Mohamedali, M.; Henni, A.; Ibrahim, H. Recent Advances in Supported Metal Catalysts for Syngas Production from Methane. *ChemEngineering* **2018**, *2*, 9. [CrossRef]

29. Dębek, R.; Motak, M.; Grzybek, T.; Galvez, M.; Da Costa, P. A Short Review on the Catalytic Activity of Hydrotalcite-Derived Materials for Dry Reforming of Methane. *Catalysts* **2017**, *7*, 32. [CrossRef]

30. Dębek, R.; Motak, M.; Galvez, M.E.; Da Costa, P.; Grzybek, T. Catalytic activity of hydrotalcite-derived catalysts in the dry reforming of methane: On the effect of Ce promotion and feed gas composition. *React. Kinet. Mech. Catal.* **2017**, *121*, 185–208. [CrossRef]

31. Liu, H.; Bel Hadjltaief, H.; Benzina, M.; Gálvez, M.E.; Da Costa, P. Natural clay based nickel catalysts for dry reforming of methane: On the effect of support promotion (La, Al, Mn). *Int. J. Hydrog. Energy* **2018**, 1–10. [CrossRef]

32. Christensen, K.O.; Chen, D.; Lødeng, R.; Holmen, A. Effect of supports and Ni crystal size on carbon formation and sintering during steam methane reforming. *Appl. Catal. A Gen.* **2006**, *314*, 9–22. [CrossRef]

33. Molina, R.; Poncelet, G. α-Alumina-Supported Nickel Catalysts Prepared from Nickel Acetylacetonate: A TPR Study. *J. Catal.* **1998**, *173*, 257–267. [CrossRef]

34. Li, C.; Chen, Y.-W. Temperature-programmed-reduction studies of nickel oxide/alumina catalysts: Effects of the preparation method. *Thermochim. Acta* **1995**, *256*, 457–465. [CrossRef]

35. Dębek, R.; Motak, M.; Duraczyńska, D.; Launay, F.; Galvez, M.E.; Grzybek, T.; Da Costa, P. Methane dry reforming over hydrotalcite-derived Ni–Mg–Al mixed oxides: The influence of Ni content on catalytic activity, selectivity and stability. *Catal. Sci. Technol.* **2016**, *6*, 6705–6715. [CrossRef]

36. Świrk, K.; Gálvez, M.E.; Motak, M.; Grzybek, T.; Rønning, M.; Da Costa, P. Yttrium promoted Ni-based double-layered hydroxides for dry methane reforming. *J. CO$_2$ Util.* **2018**, *27*, 247–258. [CrossRef]

37. Liu, H.; Wierzbicki, D.; Debek, R.; Motak, M.; Grzybek, T.; Da Costa, P.; Galvez, M.E. La-promoted Ni-hydrotalcite-derived catalysts for dry reforming of methane at low temperatures. *Fuel* **2016**, *182*, 8–16. [CrossRef]

38. Titus, J.; Goepel, M.; Schunk, S.A.; Wilde, N.; Gläser, R. The role of acid/base properties in Ni/MgO-ZrO$_2$–based catalysts for dry reforming of methane. *Catal. Commun.* **2017**, *100*, 76–80. [CrossRef]

39. Świrk, K.; Gálvez, M.E.; Motak, M.; Grzybek, T.; Rønning, M.; Da Costa, P. Syngas production from dry methane reforming over yttrium-promoted nickel-KIT-6 catalysts. *Int. J. Hydrog. Energy* **2019**, *4*, 274–286. [CrossRef]

40. Zhang, R.; Xia, G.; Li, M.; Wu, Y.; Nie, H.; Li, D. Effect of support on the performance of Ni-based catalyst in methane dry reforming. *J. Fuel Chem. Technol.* **2015**, *43*, 1359–1365. [CrossRef]

41. Świrk, K.; Rønning, M.; Motak, M.; Beaunier, P.; Da Costa, P.; Grzybek, T. Ce-and Y-modified double-layered hydroxides as catalysts for dry reforming of methane: On the effect of yttrium promotion. *Catalysts* **2019**, *9*, 56. [CrossRef]

42. Świrk, K.; Gálvez, M.E.; Motak, M.; Grzybek, T.; Rønning, M.; Da Costa, P. Dry reforming of methane over Zr- and Y-modified Ni/Mg/Al double-layered hydroxides. *Catal. Commun.* **2018**, *117*, 26–32. [CrossRef]

43. Dębek, R.; Zubek, K.; Motak, M.; Da Costa, P.; Grzybek, T. Effect of nickel incorporation into hydrotalcite-based catalyst systems for dry reforming of methane. *Res. Chem. Intermed.* **2015**, *41*, 9485–9495. [CrossRef]

44. Izquierdo-Colorado, A.; Dębek, R.; Da Costa, P.; Gálvez, M.E. Excess-methane dry and oxidative reforming on Ni-containing hydrotalcite-derived catalysts for biogas upgrading into synthesis gas. *Int. J. Hydrog. Energy* **2018**, *43*, 11981–11989. [CrossRef]

45. Kolebuk, I.; Samojeden, B. *The Preparation and Proproties of Mg-and Ni-Modified Cenospheres*; AGH University of Science and Technology: Kraków, Poland, 2018.